

# Geocoronal Solar Wind Charge Exchange Process Associated with the 2006-December-13 Coronal Mass Ejection Event

Yu Zhou<sup>1,3\*</sup>, Noriko Y. Yamasaki<sup>1,3</sup>, Shin Toriumi<sup>1</sup>, and Kazuhisa Mitsuda<sup>2,3</sup>

<sup>1</sup>Institute of Space and Astronautical Science, Japan Aerospace Exploration Agency, 3-1-1 Yoshinodai,  
Sagamihara, Kanagawa 252-5210

<sup>2</sup>National Astronomical Observatory of Japan, 2-21-1 Osawa, Mitaka, Tokyo 181-8588

<sup>3</sup>International Center for Quantum-field Measurement Systems for Studies of the Universe and Particles  
(WPI,QUP), High Energy Accelerator Research Organization, 1-1 Oho, Tsukuba, Ibaraki 300-3256

## Key Points:

- We discover a solar wind charge exchange event with Suzaku X-ray satellite driven by the 2006-December-13th coronal mass ejection.
- The SWCX occurrence time coincides with the CME magnetic cloud arrival. It is a useful knowledge in space weather forecasting.
- We modeled the light curve variation of the SWCX. The result indicates that the solar-wind flow is anisotropic in the cusp.

---

\*Current address: International Center for Quantum-field Measurement Systems for Studies of the Universe and Particles, High Energy Accelerator Research Organization, 1-1 Oho, Tsukuba, Ibaraki 300-3256

Corresponding author: Yu Zhou, [zhouyu@post.kek.jp](mailto:zhouyu@post.kek.jp)

**Abstract**

We report the discovery of a geocoronal solar wind charge exchange (SWCX) event corresponding to the well-known 2006 December 13th coronal mass ejection (CME) event. Strong evidence for the charge exchange origin of this transient diffuse emission is provided by prominent non-thermal emission lines at energies of  $O^{7+}$ ,  $Ne^{9+}$ ,  $Mg^{11+}$ ,  $Si^{12+}$ ,  $Si^{13+}$ . Especially, a 0.53 keV emission line that most likely arises from the  $N^{5+} 1s^1 5p^1 \rightarrow 1s^2$  transition is detected. Previously, the forecastability of SWCX occurrence with proton flares has been disputed. In this particular event, we found that the SWCX signal coincided with the arrival of the magnetic cloud inside CME, triggered with a time delay after the proton flux fluctuation as the CME shock front passed through the Earth. Moreover, a spacecraft orbital modulation in SWCX light curve suggests that the emission arises close to the Earth. The line of sight was found to always pass through the northern magnetospheric cusp. The SWCX intensity was high when the line of sight passed the dusk side of the cusp, suggesting an azimuthal anisotropy in the flow of solar-wind ions inside the cusp. An axisymmetric SWCX emission model is found to underestimate the observed peak intensity by a factor of about 50. We suggest this discrepancy is related to the azimuthal anisotropy of the solar-wind flow in the cusp.

**Plain Language Summary**

We discovered compelling observational evidence of the coronal mass ejection (CME) interacting with Earth’s magnetosphere by the Suzaku satellite. The signal arises from a process called charge exchange, in which heavily charged ions within the CME interact with neutral hydrogen within Earth’s magnetosphere. This specific process, known as solar wind charge exchange (SWCX), was associated with the CME event occurred on 2006 December 13th during the solar minimum. This event provided us with a unique opportunity to gain insights into the interplanetary consequences of CMEs. Despite a delay relative to the shock wave associated with the CME, the SWCX coincided with the arrival of a magnetic cloud. This suggests that solar wind ions were guided along magnetic field lines into a region near Earth called the cusp, through a process known as magnetic reconnection. Additionally, we observed that SWCX emissions were most pronounced when the satellite’s line of sight passed through the dusk region of the cusp. This indicates that the CME ejecta may have followed a path along the Parker spiral – a magnetic field pattern twisted by solar rotation – resulting in the solar wind arriving from a direction distinct from that of the Sun.

**1 Introduction**

Charge exchange (CX) process was first observed from comet Hyakutake (Lisse et al., 1996) arising from the interaction between cometary neutrals and solar wind ions (Cravens, 1997). Nowadays, we have realized that CX event can arise in various scenarios, such as the shock rim of supernova remnants (Lallement, 2009; Katsuda et al., 2011, 2012; Cumbee et al., 2014), the interface between stellar wind and surrounding interstellar medium in starburst galaxies (Pollock, 2007; Tsuru et al., 2007; J. Liu et al., 2011), merger or accretion shocks inside galaxy clusters (Walker et al., 2015; Fabian et al., 2011; Gu et al., 2015), and solar wind charge exchange (SWCX) with the planetary neutrals (Snowden et al., 2004; Cravens et al., 2003; Dennerl et al., 2006; Hui et al., 2009) and interplanetary heliosphere (Cravens, 2000; Koutroumpa et al., 2006; Galeazzi et al., 2014; Ringuette et al., 2021).

Geocoronal SWCX results from solar wind ions interacting with the neutrals in Earth’s atmosphere, leading to transient non-thermal emission lines exceeding the diffuse X-ray background spectrum (Fujimoto et al., 2007; Ezoe et al., 2010; Cravens et al., 2001; Carter & Sembay, 2008; Carter et al., 2010; Ezoe et al., 2011; Ishikawa et al., 2013; Ishi et al., 2019; Asakura et al., 2021). A significant concern in studying geocoronal SWCX events

is forecasting their occurrence through solar activity indicators. Solar wind proton flux has been observed to correlate with the charge exchange emission on timescales of about half a day (Fujimoto et al., 2007; Carter et al., 2010) or within two hours (Ezoe et al., 2011; Ishikawa et al., 2013). However, Ishi et al. (2019) demonstrates a SWCX event associated with a coronal mass ejection (CME) that lacks significant time coincidence with proton flux but instead shows a positive correlation with alpha flux.

Such complication is due to the diverse phenomena triggered by CME eruptions, including electromagnetic flares in various energy bands from radio to gamma-ray (Benz, 2017; Del Zanna & Mason, 2018), solar energetic particles (SEPs) (Desai & Giacalone, 2016), highly ionized heavy ions (Lepri & Zurbuchen, 2004; Zurbuchen & Richardson, 2006), and shock waves (Nindos et al., 2011; Verscharen et al., 2019) reaching Earth with different time delays from the solar surface. The timescales for X-ray brightening are short (minutes to hours (Shibata & Magara, 2011)), while impulsive SEP events last a few hours, and large-scale gradual SEP events can persist for several days (Reames, 1999; Desai & Giacalone, 2016). Solar wind (SW), categorized as slow wind (approximately  $400 \text{ km s}^{-1}$ ), fast wind (around  $700\text{-}800 \text{ km s}^{-1}$ ), and coronal mass ejections (CMEs) with speeds up to  $2000 \text{ km s}^{-1}$ , approaches Earth over several days or weeks (McComas et al., 1998; Viall & Borovsky, 2020; Verscharen et al., 2019). This makes it challenging to establish clear correlations between different tracers, especially during frequent solar flares.

Modeling the SWCX spectrum is another challenge, considering uncertainties in the CX cross section, ionic composition of the solar wind, relative velocity between solar wind and neutrals, and the SWCX interaction geometry with the magnetosphere.

Theoretical approaches to calculate the CX cross section include quantum-mechanical methods (Nolte et al., 2012), atomic-orbital close-coupling (Fritsch & Lin, 1991), classical trajectory Monte Carlo (Abrines & Percival, 1966; Olson & Salop, 1977), and multi-channel Landau-Zener method (Janev & Winter, 1985). However, laboratory measurements of the CX cross section are limited to a small number of ions (Fite et al., 1962; Meyer et al., 1979, 1985; Crandall et al., 1979; Ali et al., 2005; Wargelin et al., 2005; Greenwood et al., 2000; Defay et al., 2013; Fogle et al., 2014; Beiersdorfer et al., 2003; Mullen et al., 2017, 2016; Cumbee et al., 2018). Consequently, integrated astronomical data analysis software often relies on scaling relations (Gu et al., 2016; Olson & Salop, 1977) or empirical formulae to estimate these values (Smith et al., 2012).

The SW ionic composition and velocity are determined by factors such as the solar flare temperature, plasma equilibrium state at the moment it becomes collisionless, acceleration and release mechanisms (Viall & Borovsky, 2020), as well as deceleration during propagation and the first ionization potential fractionation status under ponderomotive forces induced by magneto-hydrodynamic waves (Laming, 2015). If SW velocity and CX cross section are accurately constrained, the SWCX spectrum observation can serve as a remote sensor for highly ionized ions in the solar wind, complementing in-situ ion composition spectrometers (Gloeckler et al., 1998).

The poorly understood geometry of the geocoronal SWCX interaction is also a critical aspect. Studies often assume that solar wind ions fill the magnetosheath, with further penetration resisted by magnetic pressure at the magnetopause (Ezoe et al., 2011; Carter et al., 2010; Ishikawa et al., 2013; Ishi et al., 2019). However, magnetohydrodynamic (MHD) simulations show prominent X-rays from CX collisions between solar wind ions and Earth's exospheric neutrals in the cusp region (Robertson et al., 2006). Observations by Suzaku, pointing towards the North pole, indicated that X-ray intensity variation is anti-correlated with the geocentric distance from the point where the geomagnetic field first opens to space, suggesting SWCX emission can penetrate deeper than the magnetosheath near the cusp region (Fujimoto et al., 2007).

In this study, we present a unique case of geocoronal SWCX observed by the Suzaku satellite, associated with a well-distinguished source CME occurring on December 13th, 2006. The solar environment was near solar minimum at the time, minimizing contamination from other events and offering a valuable opportunity to study the space weather consequences of the CME. Especially, the satellite's line-of-sight was directed towards the North pole which allows a cusp observation. Section 2 provides a comprehensive background description of in-situ measurements for this CME event. Section 3 describes the data reduction details for Suzaku observations. We report the SWCX spectrum detected by Suzaku in section 4 and explore the time coincidences with interplanetary and Earth magnetic fields in section 5. Furthermore, we discuss the SWCX geometry modeling in section 6. Summary and conclusion are given in section 7.

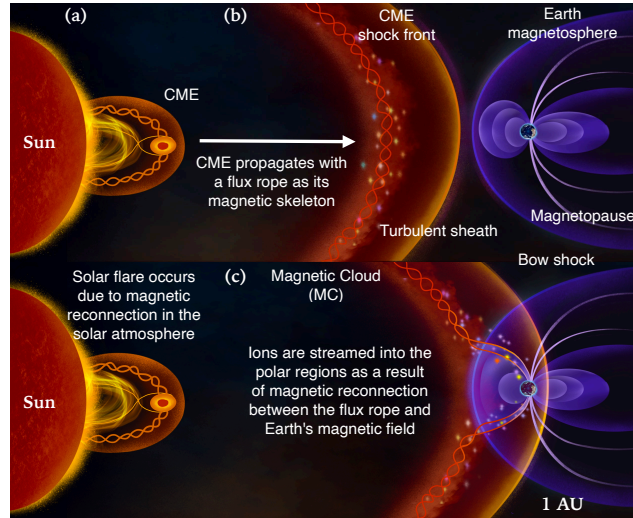


**Figure 1.** A schematic of the CME propagation. (a) Initially, the solar flare occurs and the CME is launched near the solar surface as a result of magnetic reconnection, which is observed (in part) as abrupt enhancements of soft X-ray and proton flux (Zurbuchen & Richardson, 2006; Shibata & Magara, 2011). (b) The CME propagates the interplanetary space (ICME) towards the Earth with the magnetic flux rope as its core. The turbulent sheath forms behind the CME shock front and reaches the Earth in advance of the MC. (c) As a result of reconnection between the flux rope and Earth's magnetic field, the heavily ionized ions are streamed into the magnetosphere, particularly to the polar regions, along the magnetic field lines. The artistic drawing is contributed by courtesy of designer Xuelei Chuai.

## 2 CME Event on 2006 December 13

The CME event that occurred on 2006 December 13 was one of the largest halo CMEs since the intense solar activity in 2003. This CME was associated with the X3.4-class solar flare, emanating from NOAA active region 10930, which was accompanied by the radio bursts, SEP event, and MC passage. This flare event has been studied in detail from both observational and theoretical points of view, which is summarized in Hinode Review Team et al. (2019) and Toriumi and Wang (2019).

The coronal observations from the Large Angle Spectroscopic Coronagraph and the Extreme ultraviolet Imaging Telescope aboard the Solar and Heliospheric Observatory shows a strong EUV brightening at 02:30 UT, followed by a dimming and forming into a ring of dense material around 03:06 UT (Y. Liu et al., 2008). The CME initial veloc-

ity is  $1774 \text{ km s}^{-1}$  near the Sun according to the coronagraph height-time observation. After the abrupt formation, the CME ejecta propagates into the space and its interplanetary CME (ICME) consequences, including low-energy and high-energy electrons, protons, MC, were measured in-situ by the *STEREO* and *ACE* satellite at 1 AU (Mewaldt et al., 2008). At 14:38 UT on December 14, about 36 hours later than the CME outburst, a preceding shock passed the spacecraft at an average speed of  $\sim 1160 \text{ km s}^{-1}$  as suggested by simultaneous enhancements in the electron flux and magnetic field strength. This speed has decreased compared with the initial velocity near the Sun but larger than the shock speed as calculated according to mass conservation across the shock at 1 AU ( $\sim 1030 \text{ km s}^{-1}$ ) (Y. Liu et al., 2008). Following the preceding shock and magnetic fluctuation period, the detected magnetic field shows clear rotation, indicating that spacecraft seems to cross the MC interior (Y. Liu et al., 2008; Kataoka et al., 2009). The shock downstream of the ICME was detected later on 17:23 UT on December 16 with a sharp but short duration jump in the proton flux and magnetic field strength. The shock was finally detected by the *Ulysses* with a speed of  $870 \text{ km s}^{-1}$  at a distance of 2.73 AU to the Sun and to the  $117^\circ$  east and  $74^\circ$  south of the Earth at 17:02 UT on December 17 (Richardson et al., 2005). But other signatures of ICME, such as enhanced helium abundances, decreased proton temperature, or smooth strong magnetic fields were not detected at *Ulysses*.

### 3 SWCX event captured by Suzaku Observations

We analysed the *Suzaku* observations that covers the time period since CME formation to its passage across the Earth, including two individual datasets with ObsIDs 801032010 and 701060010.

#### 3.1 observation 801032010

The observation (obsID:801032010) was originally targeted on the galaxy cluster Abell 1555, with a few point-sources discernable in the 0.5-2 keV image, as shown in Figure 2 (a). The exposure time of observation, from 2006-Dec-12 22:16 UT to 2006-Dec-13 18:38 UT, has covered the CME-accompanied X3.4 flare at 2006-Dec-13 02:14 UT and enabled a tracking of detector response since the onset of solar flare.

We select the background region to exclude any contribution from the discrete sources and extract the light curve and energy spectrum of the diffuse background. No significant flare is observed in the light curve of the dark sky data (selected with the criteria  $\text{ELV} > 5$  &  $\text{DYE\_ELV} > 20$  &  $\text{SUN\_ALT} < 0$ ) except for a moderate orbital modulation around the solar flare phase. But the sunlit Earth phase data (selected with the criteria  $\text{ELV} < 0$  &  $\text{SUN\_ALT} > 0$ ) has shown significant enhancement during the solar flare period near 02:14 UT on 2006 December 13, which reflects the solar flare photons scattered in the Earth atmosphere. We further divided the light curve of the flare period into small segments and found an abrupt emergence of line emission at  $\sim 1.5 \text{ keV}$  (indicated as [D] period in Figure 4 (b), and the spectrum shown in Figure 2 (b). Confirming that the decay time constant of the 1.5 keV line is comparable to that of the solar flare X-ray fluxes in 1-8 Å energy range, rather than that of the proton fluxes detected by GOES satellite, we conclude that this line emission is originated from the fluorescent instrumental Al  $K\alpha$  line (1.486 keV) created by secondary X-ray photons scattered inside the telescope.

Besides, *Suzaku* detected an excess of blended line emissions in the 3-7 keV energy range during the solar flare period, which are probably originated from solar flare photons diffusely reflected by the Earth atmosphere that were partially collected by the telescope. The line emission at 6.62 keV prominent enough to be recognized as highly ionized Fe XXV line, which is also seen in the Earth albedo spectrum extracted from the sunlit Earth data, supports this conjecture.

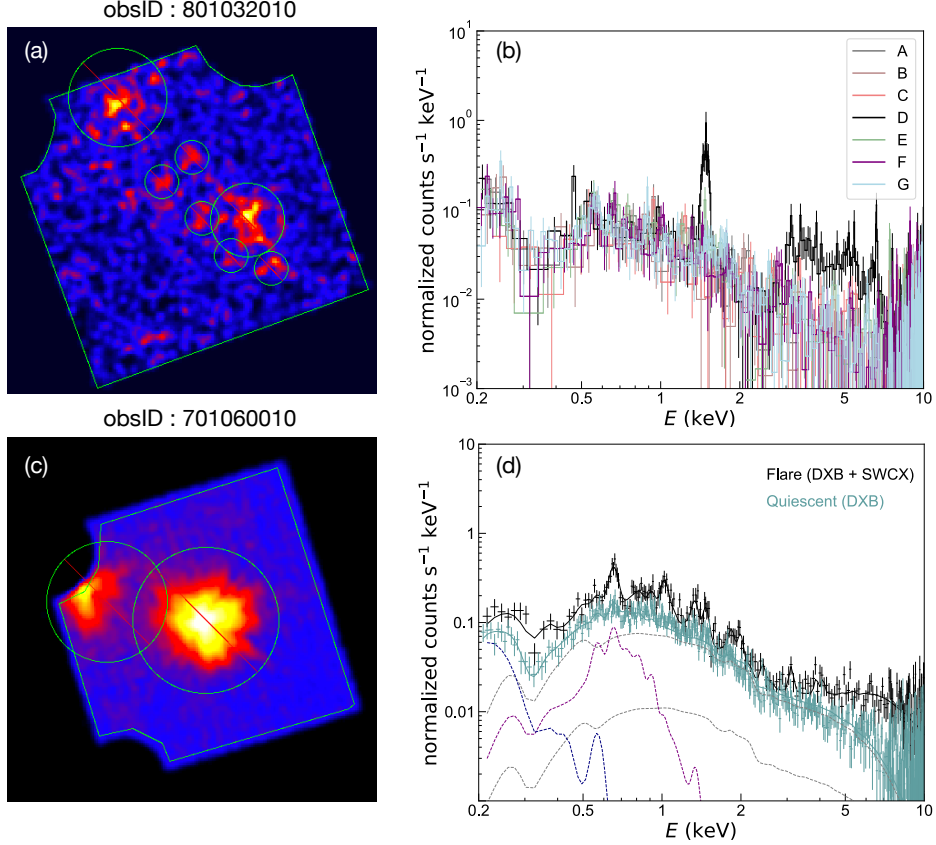


**Figure 2.** (a) and (b) shows the images of the observation 801032010 and 701060010. The green frames enclose the CDD regions where the energy spectra were extracted from. (c): Energy spectra for the observation 801032010, generated separately for the time intervals [A-G] defined from the light curves shown in Figure 4 (b). (d): Energy spectra for the observation 701060010 that compare the quiescent and flare time periods defined from the light curves shown in Figure 4 (d). Models fitting to the diffuse X-ray background break down to three major components: unresolved point sources in the cosmic X-ray background (gray dashed lines), hot plasma in the galactic gaseous halo (purple dashed line), and warm-hot gas in the local hot bubble (blue dashed line).

### 3.2 observation 701060010

The observation (obsID:701060010) was pointed towards a Seyfert 1 galaxy, 3C 390.3, with two bright sources in the field of view, as shown in the full-band image in Figure 2 (c). The timespan of the observation is from 2006-Dec-14 03:25 UT to 2006-Dec-16 03:19 UT, which contains the time period when the ICME shock and MC passed by the Earth at around 2006-Dec-14 14:38 UT. We also noticed an X1.5 flare detected by GOES starting from 22:07 UT on December 14 (see Figure 4 (d)).

We select only the background region to extract the light curve and energy spectrum of the diffuse X-ray background emission. As seen in Figure 4 (d), the light curve of Suzaku dark sky between 2006-Dec-15 0h and 6h shows significant orbital modulation during the flare phase with a higher count rates at maxima compared to the quiescent phase. A spectral excess is also clearly observed in the flare phase in comparison



with the spectrum of the quiescent state. The excess emission is dominated by individual lines in 0.5-2 keV energy range.

All four *Suzaku* XIS detectors have sensed the transient SWCX excess emission during the flare state. We extracted the energy spectra during the flare and quiescent periods for both back-side and front-side illuminated CCD detectors. We merged the spectra for the front-side illuminated sensor XIS0, XIS2, and XIS3 to obtain a spectrum with higher signal-to-noise ratio. The corresponding response files, ancillary files, and non-X-ray background files were also combined using the ASCA `ftool` command `addascaspec`. The energy spectra extracted in the quiescent period were finally subtracted from the source spectra to exhibit the charge exchange excess for further modelling of the net SWCX spectrum. The net SWCX spectra after background subtraction for both types of CCDs are shown in Figure 3 (a).

#### 4 Geocoronal SWCX energy spectrum

Figure 3 shows the SWCX energy spectrum fitted with multiple models for both front-side and back-side illuminated CCDs. Table 1 shows the fitted centroid energies and flux of the emission lines and their probable identifications. We found that excess emission lines with fitted centroid energies around 0.652 keV ( $O^{7+}$ ), 1.02 keV ( $Ne^{9+}$ ), 1.32 keV ( $Ne^{9+}$ ), 1.47 keV ( $Mg^{11+}$ ), 1.86 keV ( $Si^{12+}$ ), and 1.97 keV ( $Si^{13+}$ ) are typically seen in the observed geocoronal SWCX spectrum. Specially, we observed an unusual emission line at about 0.53 keV. It is most likely the  $N^{5+} 1s^1 5p^1 \rightarrow 1s^2$  transition which provides a strong evidence that the excess emission is of a non-thermal origin. Another possibility is that there is fluorescent emission of O  $K\alpha$  line at 0.525 keV reflected inside the Earth atmosphere. However, we do not observe comparable amount of N  $K\alpha$  line at 0.392 keV which is another fluorescent line expected to emerge as seen in the Earth albedo spectrum. Therefore, the 0.53 keV line is not very likely to arise from the Earth atmosphere fluorescence. Besides, the emission around  $\sim 0.8$  keV has a broad energy distribution and has been usually recognized as the Fe-L shell complex. The fit with CX models, however, suggested that this bump at  $\sim 0.8$  keV is possibly contributed by oxygen (see Figure 3 (b)-1 and (c)-1). Another point worthy of discussion is the 1.32 keV  $Ne^{9+}$  line, around this energy the line could also be recognized as 1.329 keV  $Mg^{10+}$ , whereas the CX model favors to fit the 1.32 keV line with  $Ne^{9+}$ .

In Table 1 we show the best-fitted temperature and metal abundances with the CX model in SPEX and XSPEC. Both models are based on the collisional ionization equilibrium assumption, which may not hold for rapidly expanding CME plasmas that have not reached the equilibrium state when becoming collisionless. The fit results show significant degeneracies among the temperature, velocity, and metal abundances in SPEX-CX model. The XSPEC-VACX2 model suggests a larger collisional velocity, or higher element abundance ratio to oxygen for heavier ions than SPEX-CX model.

#### 5 SWCX as a result of the interaction between the interplanetary and Earth magnetic field

We found two observational evidences suggesting that the observed SWCX emission is associated with the interplanetary and Earth magnetic field: (1) A time coincidence between the arrival of the magnetic cloud (MC) and the SWCX occurrence. (2) An orbital modulation in SWCX light curve.

Figure 4 shows the light curves of the soft X-ray and proton flux detected by GOES, and magnetic field strength, alpha to proton density ratio, and proton density measured in-situ by ACE, together with the SWCX emission detected by Suzaku. The SWCX flaring starts around 2006-Dec-15th 00:00 UT, which is right after the ACE magnetic field strength entering a smooth transition phase, indicating the passage of an MC (Y. Liu

**Table 1.** Model fit parameters for SWCX spectrum

| Model            | Energy<br>(eV)                         | Line Identification  | Surface Brightness<br>(photons cm <sup>-2</sup> s <sup>-1</sup> str <sup>-1</sup> ) | Flux ratio to O <sup>7+</sup>  |
|------------------|--|--|---|--------------------------------|
| Gaussian         | 530 <sup>+4</sup> <sub>-15</sub>       | N <sup>5+</sup> 1s <sup>1</sup> 5p <sup>1</sup> → 1s <sup>2</sup> (533 eV)   | 2.4 <sup>+0.5</sup> <sub>-0.5</sub>   | 0.42                           |
|                  | 647 <sup>+5</sup> <sub>-4</sub>        | O <sup>7+</sup> 2p <sup>1</sup> → 1s <sup>1</sup> (653 eV)   | 5.7 <sup>+0.6</sup> <sub>-0.6</sub>   | 1                              |
|                  | 813 <sup>+16</sup> <sub>-29</sub>      | Fe <sup>16+</sup> 2p <sup>5</sup> 3d <sup>1</sup> → 2p <sup>6</sup> (826 eV, 812 eV)   | 2.6 <sup>+0.4</sup> <sub>-0.4</sub>   | 0.46                           |
|                  | 1028 <sup>+5</sup> <sub>-4</sub>       | Ne <sup>9+</sup> 2p <sup>1</sup> → 1s <sup>1</sup> (1.022 keV)   | 1.39 <sup>+0.18</sup> <sub>-0.18</sub>  | 0.24                           |
|                  | 1089 <sup>+67</sup> <sub>-87</sub>     | Fe <sup>23+</sup> 1s <sup>2</sup> 3s <sup>1</sup> → 1s <sup>2</sup> 2p <sup>1</sup> (1.085 keV), Fe <sup>17+</sup> , Fe <sup>21+</sup>   | 1.1 <sup>+0.2</sup> <sub>-0.2</sub>   | 0.19                           |
|                  | 1320 <sup>+9</sup> <sub>-10</sub>      | Ne <sup>9+</sup> 6p <sup>1</sup> → 1s <sup>1</sup> (1.324 keV)   | 0.57 <sup>+0.10</sup> <sub>-0.10</sub>  | 0.10                           |
|                  | 1460 <sup>+6</sup> <sub>-5</sub>       | Mg <sup>11+</sup> 2p <sup>1</sup> → 1s <sup>1</sup> (1.472 keV)  | 0.8 <sup>+0.1</sup> <sub>-0.1</sub>   | 0.14                           |
|                  | 1857 <sup>+23</sup> <sub>-22</sub>     | Si <sup>12+</sup> 1s <sup>1</sup> 2p <sup>1</sup> → 1s <sup>2</sup> (1.865 keV)  | 0.6 <sup>+0.2</sup> <sub>-0.2</sub>   | 0.10                           |
|                  | 1973 <sup>+26</sup> <sub>-36</sub>     | Si <sup>13+</sup> 2p <sup>1</sup> → 1s <sup>1</sup> (2.006 keV)  | 0.2 <sup>+0.1</sup> <sub>-0.1</sub>   | 0.035                          |
|                  | Model                                  | kT (keV)   | Abundance   | Velocity (km s <sup>-1</sup> ) |
| CX<br>(SPEX)     | 1.04 <sup>+0.01</sup> <sub>-0.01</sub> | Solar abundance <sup>†</sup>   | 592 <sup>+113</sup> <sub>-56</sub>  | 4.54                           |
|                  | 1.14 <sup>+0.02</sup> <sub>-0.02</sub> | C/C <sub>⊙</sub> = 8.2 <sup>+0.9</sup> <sub>-0.9</sub> N/N <sub>⊙</sub> = 6.7 <sup>+0.7</sup> <sub>-0.6</sub>  | 232 <sup>+45</sup> <sub>-25</sub>   | 4.16                           |
| VACX2<br>(XSPEC) | 1.16                                   | Ne/Ne <sub>⊙</sub> = 0.8 <sup>+0.05</sup> <sub>-0.05</sub> Mg/Mg <sub>⊙</sub> = 0.91 <sup>+0.08</sup> <sub>-0.07</sub> Si/Si <sub>⊙</sub> = 0.43 <sup>+0.07</sup> <sub>-0.06</sub> | 448.617   | 3.62                           |
|                  | 1.05                                   | Solar abundance<br>C/C <sub>⊙</sub> = 3.67245 N/N <sub>⊙</sub> = 5.26688<br>Ne/Ne <sub>⊙</sub> = 1.90699 Mg/Mg <sub>⊙</sub> = 4.15255 Si/Si <sub>⊙</sub> = 1.78754                 | 854.947   | 3.22                           |

<sup>†</sup> Solar abundance refers to the abundance in the solar photosphere (Anders & Grevesse, 1989).



et al., 2008). Before the MC phase, ACE also detected significant fluctuation in the field strength and the proton density between 14:00 to 24:00 UT on 2006-Dec-14th, corresponding to the turbulent sheath of the CME shock front. This is consistent with the CME propagation in the standard flare model illustrated in Figure 1, in which the magnetic reconnection between the coronal loops launches a CME with a magnetic flux rope as its skeleton. When arriving at the Earth, the flux rope and Earth field could reconnect so that the heavily ionized ions are streamed into the magnetosphere, particularly to the polar regions, along the magnetic field lines.

Furthermore, we find that the X-ray background intensity has a significant time variation associated with the satellite orbital motion during the SWCX occurrence period, shown in Figure 6 (a). We reason that this time variation indicates that the source emission region is located close to the observer. Assuming the source distance is  $D$ , the maximum physics size the telescope can observe within the field of view (FoV with angular size  $\theta$ ) is  $D\theta$ . Having witnessed the time variation of the diffuse emission suggests the source moves in and out of the telescope FoV as satellite orbits around and the source region extension must be smaller than the orbit diameter  $2R_{\text{orb}}$ . The distance is thus constrained to be  $D < 2R_{\text{orb}}/\theta = 370R_{\text{E}}$ , where  $R_{\text{E}}$  is the diameter of the Earth on the equator plane. Given that the observation was pointed towards the direction of the North pole, it is likely that the line of sight passed through the cusp region of the Earth's magnetic field. We define the  $r_{\text{mp}}$  as the geocentric distance of the point where geomagnetic field becomes open to space for the first time along the line of sight starting from the spacecraft, and estimate  $r_{\text{mp}}$  using Tsyganenko geomagnetic field (T96) model (Tsyganenko, 1995; Tsyganenko & Sitnov, 2005) and geopack libraries. Figure 5 shows a sketch of the  $r_{\text{mp}}$  definition related to the magnetosphere geometry. The solar wind ram pressure is chosen to be 4.3 nPa, with the proton density  $3.59 \text{ cm}^{-3}$  and proton velocity  $846.52 \text{ km s}^{-1}$  as measured by ACE, and the interplanetary magnetic field strength of  $B_y \sim 11 \text{ nT}$  and  $B_z \sim -13 \text{ nT}$ , and  $Dst$  index  $\sim -153 \text{ nT}$  adopted as the input parameters of the model.

As shown in Figure 6 (a),  $r_{\text{mp}}$  is in the range of 1.5 to  $\sim 3R_{\text{E}}$ , which is much smaller than the outer boundary of Earth magnetosphere,  $10 R_{\text{E}}$ , throughout the whole orbit period, suggesting the satellite line of sight passed through the cusp region. The strong SWCX emission could be explained by the penetration of solar-wind ions to the cusp region (Walsh et al., 2016) where the neutral hydrogen density is high, with the solar wind being resisted to penetrate into any deeper region below  $r_{\text{mp}}$  due to the strong magnetic pressure. If the neutral hydrogen density is the dominant factor determining the SWCX intensity, the maximum emission is expected at the lowest  $r_{\text{mp}}$  point, which is, however, not the case. On the other hand, variation in solar wind ion density dominated by gravity-pressure balance in the ionosphere is less likely to account for the SWCX intensity orbital dependence, either, since the solar wind will stop falling below the ionosphere boundary  $\sim 2.5R_{\text{E}}$ . Therefore, radial variation in neutral hydrogen or solar wind ion density cannot account for the observed light curve and another mechanism is necessary. Azimuthal solar wind ion intensity non-uniformity inside the cusp region provides one possible solution. In Figure 6 (b), we plot the X-ray intensity and  $r_{\text{mp}}$  as functions of the azimuthal angle of the  $r_{\text{mp}}$  position in GSM (geocentric solar magnetospheric coordinates) for the second orbital cycle, showing that the SWCX intensity is high when the satellite line of sight passes through the dusk side of the cusp, which means an azimuthal asymmetry exist in the solar wind density distribution in the cusp. Such density gradient may be related to the Parker spiral-type propagation of solar wind enhancement in the planetary space (Koutroumpa et al., 2007) in which scenario the solar wind enhancement due to a CME event first arrives from the dusk side of the Earth. However, the azimuthal angle of the hit point in GSM is likely  $< 90^\circ$ , while the peak of the X-ray intensity is at  $\sim 130^\circ$ . We consider it is necessary to model solar wind transportation with azimuthal non-uniformity in the cusp.

## 6 Modelling the orbital modulation of the SWCX count rate

The surface brightness of SWCX,  $S$  is estimated by integrating the emission intensity per volume along the line of sight  $s$ ,

$$S = \frac{1}{4\pi} \int_{s_0}^{s_1} \alpha n_{\text{H}}(s) n_{\text{ion}}(s) v_{\text{col}} ds. \quad (1)$$

Then the observed intensity,  $R$ , is obtained by convolving  $S$  with the telescope and detector response functions, and is approximately,  $R = A\Omega S$ , where  $A$  and  $\Omega$  are, respectively, the effective area and the field of view of the instrument. For CX emission line of certain ions, for example,  $O^{8+}$ , the ion density is estimated by solar wind ion density and ionic abundance,  $n_{\text{ion}} = n_{\text{sw}} \chi_{O^{8+}}$ .

$v_{\text{col}}$  is the relative collisional speed between solar wind ions and neutral atoms in the Earth atmosphere. Here we assume  $v_{\text{col}} = 500 \text{ km s}^{-1}$ , a speed smaller than the 1 AU speed of the CME shock,  $\sim 1030 \text{ km s}^{-1}$  (Y. Liu et al., 2008), and neglect the thermal velocity. The charge exchange cross section,  $\alpha$ , is chosen as  $5 \times 10^{-15} \text{ cm}^2$  for  $O^{8+} + H$  collisions at  $v_{\text{col}} = 500 \text{ km s}^{-1}$  (Lee et al., 2004; Kimura & Lane, 1987).

The neutral hydrogen density along line-of-sight  $n_{\text{H}}(s)$  is a function of the position in the Earth coordinate, which, more specifically, is a function the distance from the Earth center, i.e.  $n_{\text{H}}(s) = n_{\text{H}}(r(s))$ . We use the geocoronal model proposed by ØStgaard et al. (2003) as an approximation to the neutral hydrogen density distribution in the Earth atmosphere,  $n_{\text{H}}(r) = 10000e^{-r/1.02} + 70e^{-r/8.2}$ , where  $r$  is in the unit of  $R_{\text{E}}$  and  $n_{\text{H}}(r)$  in the unit of  $\text{cm}^{-3}$ . The model is based on the measurements of the Lyman  $\alpha$  column brightness by the Geocoronal Imager on board the IMAGE satellite at high altitudes ( $> 3.5 R_{\text{E}}$ ) where the neutral hydrogen is considered as an optical thin medium. Our estimation of neutral hydrogen density may suffer from large uncertainty due to the following reasons: (1) The variation of solar Lyman  $\alpha$  flux itself from solar minimum to solar maximum is about a factor of 1.5 on average to 2.1 maximum; (2) We extrapolate the empirical model to smaller altitudes where the medium is no longer optically thin and more complex analysis including radiative transfer is required; (3) Asymmetric exosphere, "magnetotail", may present higher densities at high altitudes in the night-side than day-side direction under the radiation pressure.

The solar-wind ion density,  $n_{\text{sw}}(s)$ , is also a function of the position in the Earth coordinate. Walsh et al. (2016) showed the ion density as a function of the distance from the Earth center using numerical simulations. Their result shows that the density drops from  $\sim 9R_{\text{E}}$  to  $\sim 6R_{\text{E}}$ , and stays constant down to  $\sim 2.5R_{\text{E}}$ , then becomes zero. According to ACE satellite we found the proton density of the CME shock peaked around  $15 \text{ cm}^{-3}$ . We thus normalize the  $n_{\text{sw}}(s)$  at the outer boundary of the magnetosphere to be  $15 \text{ cm}^{-3}$  and use the radial profile in Walsh et al. (2016) as the solar-wind ion density radial dependence along line of sight in our model. As discussed in the previous section, we need to introduce density gradient from sun side to anti-sun side with in the cusp. We have no physical model for this, though. We thus assume a simple toy model, in which the density is also a function of  $\Theta$  defined in the previous section,  $n_{\text{ion}}(s) = n_{\text{ion}}(r(s), \Theta(s))$ . The solar-wind ion density orbital modulation function is defined as  $f(\Theta) = M e^{-\frac{1}{2} \frac{(\Theta - \mu)^2}{\sigma^2}}$ , where  $\mu = 0.5$ ,  $\sigma = 0.5$ , and  $M$  is a normalization factor.  $\mu$  is chosen to be 0.5 such that the solar-wind density is the highest when the satellite moves closest to the sun. The abundance of  $O^{8+}$  ions is estimated as its photospheric value,  $8.51 \times 10^{-4}$  (Anders & Grevesse, 1989).

With the assumptions discussed above, the model predicts  $O^{7+}$  the count rate to be  $0.01 \text{ cts s}^{-1}$ . On the other hand, from the energy spectrum, we estimate the observed  $O^{7+}$  count rate at the peak of figure 6 (a) to be  $\sim 0.5 \text{ cts s}^{-1}$ , which exceeds the model predication by a factor about 50. This large discrepancy could be related the non-uniformity of the flow in the cusp region as discussed in section 5. If the plasma flow is confined in

1/50 of the whole cusp volume, the density is likely enhanced by this factor compared to the prediction with the uniform model from Walsh et al. (2016). In figure 6 (b), the FWHM of the peak is about 0.8 radian, which is about 1/8 of  $2\pi$ . A factor of 50 times change in volume can be explained if the plasma is compressed in two directions with this ratio.

## 7 Summary and conclusion

We report an unique case of SWCX event caused by the well-known 2006-December-13 CME, which is captured by Suzaku observation with a line-of-sight cutting through the cusp region. Significant non-thermal emission lines from  $O^{7+}$ ,  $Ne^{9+}$ ,  $Mg^{11+}$ ,  $Si^{12+}$ ,  $Si^{13+}$ , and probably,  $N^{5+} 1s^1 5p^1 \rightarrow 1s^2$  transition are detected and we fit the SWCX spectrum with CX models. We find a time coincidence between the arrival of CME magnetic cloud and the SWCX occurrence, suggesting that the solar wind ions can be streamed onto the Earth field lines via magnetic reconnection. The time variation of the X-ray emission suggests non-uniformity of the solar wind flow in the cusp region which enhances the X-ray surface brightness by a factor of  $\sim 50$ . The SWCX is bright in the dusk side of the cusp and we conjecture that this is related to the Parker spiral-type propagation of the solar wind.

## Open Research Section

Suzaku archive data available from the DARTS/Suzaku Public Data list ([https://data.darts.isas.jaxa.jp/pub/Astro\\_Browse/publications/suzaku/public\\_list.html](https://data.darts.isas.jaxa.jp/pub/Astro_Browse/publications/suzaku/public_list.html)) were used in the creation of this manuscript. The Tsyganenko Geomagnetic Field Model and GEOPACK libraries are published on Github <https://github.com/tsssss/geopack>.

## Acknowledgments

We thank professor Hiroya Yamaguchi and Yuichiro Ezoe for insightful discussions and KAKENHI grants: JP20KK0072 (PI: S. Toriumi), JP21H01124 (PI: T. Yokoyama), and JP21H04492 (PI: K. Kusano).

## References

- Abrines, R., & Percival, I. C. (1966, August). Classical theory of charge transfer and ionization of hydrogen atoms by protons. *Proceedings of the Physical Society*, 88(4), 861-872. doi: 10.1088/0370-1328/88/4/306
- Ali, R., Neill, P. A., Beiersdorfer, P., Harris, C. L., Raković, M. J., Wang, J. G., ... Stancil, P. C. (2005, August). On the Significance of the Contribution of Multiple-Electron Capture Processes to Cometary X-Ray Emission. *The Astrophysical Journal Letter*, 629(2), L125-L128. doi: 10.1086/447768
- Anders, E., & Grevesse, N. (1989, January). Abundances of the elements: Meteoritic and solar. *Geochimica et Cosmochimica Acta*, 53(1), 197-214. doi: 10.1016/0016-7037(89)90286-X
- Asakura, K., Matsumoto, H., Okazaki, K., Yoneyama, T., Noda, H., Hayashida, K., ... Ezoe, Y. (2021, June). Suzaku detection of solar wind charge exchange emission from a variety of highly ionized ions in an interplanetary coronal mass ejection. *Publications of the Astronomical Society of Japan*, 73(3), 504-518. doi: 10.1093/pasj/psab015
- Beiersdorfer, P., Boyce, K. R., Brown, G. V., Chen, H., Kahn, S. M., Kelley, R. L., ... Tillotson, W. A. (2003, June). Laboratory Simulation of Charge Exchange-Produced X-ray Emission from Comets. *Science*, 300(5625), 1558-1560. doi: 10.1126/science.1084373

- Benz, A. O. (2017, December). Flare Observations. *Living Reviews in Solar Physics*, *14*(1), 2. doi: 10.1007/s41116-016-0004-3
- Carter, J. A., & Sembay, S. (2008, October). Identifying XMM-Newton observations affected by solar wind charge exchange. Part I. *Astronomy and Astrophysics*, *489*(2), 837-848. doi: 10.1051/0004-6361:200809997
- Carter, J. A., Sembay, S., & Read, A. M. (2010, February). A high charge state coronal mass ejection seen through solar wind charge exchange emission as detected by XMM-Newton. *Monthly Notices of the Royal Astronomical Society*, *402*(2), 867-878. doi: 10.1111/j.1365-2966.2009.15985.x
- Crandall, D. H., Phaneuf, R. A., & Meyer, F. W. (1979, February). Electron capture by slow multicharged ions in atomic and molecular hydrogen. *Physical Review A*, *19*(2), 504-514. doi: 10.1103/PhysRevA.19.504
- Cravens, T. E. (1997, January). Comet Hyakutake x-ray source: Charge transfer of solar wind heavy ions. *Geophysical Research Letters*, *24*(1), 105-108. doi: 10.1029/96GL03780
- Cravens, T. E. (2000, April). Heliospheric X-ray Emission Associated with Charge Transfer of the Solar Wind with Interstellar Neutrals. *The Astrophysical Journal Letter*, *532*(2), L153-L156. doi: 10.1086/312574
- Cravens, T. E., Robertson, I. P., & Snowden, S. L. (2001, November). Temporal variations of geocoronal and heliospheric X-ray emission associated with the solar wind interaction with neutrals. *Journal of Geophysical Research*, *106*(A11), 24883-24892. doi: 10.1029/2000JA000461
- Cravens, T. E., Waite, J. H., Gombosi, T. I., Lugaz, N., Gladstone, G. R., Mauk, B. H., & MacDowall, R. J. (2003, December). Implications of Jovian X-ray emission for magnetosphere-ionosphere coupling. *Journal of Geophysical Research (Space Physics)*, *108*(A12), 1465. doi: 10.1029/2003JA010050
- Cumbee, R. S., Henley, D. B., Stancil, P. C., Shelton, R. L., Nolte, J. L., Wu, Y., & Schultz, D. R. (2014, June). Can Charge Exchange Explain Anomalous Soft X-Ray Emission in the Cygnus Loop? *The Astrophysical Journal Letter*, *787*(2), L31. doi: 10.1088/2041-8205/787/2/L31
- Cumbee, R. S., Mullen, P. D., Lyons, D., Shelton, R. L., Fogle, M., Schultz, D. R., & Stancil, P. C. (2018, January). Charge Exchange X-Ray Emission due to Highly Charged Ion Collisions with H, He, and H<sub>2</sub>: Line Ratios for Heliospheric and Interstellar Applications. *The Astrophysical Journal*, *852*(1), 7. doi: 10.3847/1538-4357/aa99d8
- Defay, X., Morgan, K., McCammon, D., Wulf, D., Andrianarijaona, V. M., Fogle, M., ... Havener, C. C. (2013, November). X-ray emission measurements following charge exchange between C<sup>6+</sup> and He. *Physical Review A*, *88*(5), 052702. doi: 10.1103/PhysRevA.88.052702
- Del Zanna, G., & Mason, H. E. (2018, August). Solar UV and X-ray spectral diagnostics. *Living Reviews in Solar Physics*, *15*(1), 5. doi: 10.1007/s41116-018-0015-3
- Dennerl, K., Lisse, C. M., Bhardwaj, A., Burwitz, V., Englhauser, J., Gunell, H., ... Rodríguez-Pascual, P. M. (2006, May). First observation of Mars with XMM-Newton. High resolution X-ray spectroscopy with RGS. *Astronomy and Astrophysics*, *451*(2), 709-722. doi: 10.1051/0004-6361:20054253
- Desai, M., & Giacalone, J. (2016, September). Large gradual solar energetic particle events. *Living Reviews in Solar Physics*, *13*(1), 3. doi: 10.1007/s41116-016-0002-5
- Ezoe, Y., Ebisawa, K., Yamasaki, N. Y., Mitsuda, K., Yoshitake, H., Terada, N., ... Fujimoto, R. (2010, August). Time Variability of the Geocoronal Solar-Wind Charge Exchange in the Direction of the Celestial Equator. *Publications of the Astronomical Society of Japan*, *62*, 981. doi: 10.1093/pasj/62.4.981
- Ezoe, Y., Miyoshi, Y., Yoshitake, H., Mitsuda, K., Terada, N., Oishi, S., & Ohashi, T. (2011, November). Enhancement of Terrestrial Diffuse X-Ray Emis-

- sion Associated with Coronal Mass Ejection and Geomagnetic Storm. *Publications of the Astronomical Society of Japan*, 63, S691-S704. doi: 10.1093/pasj/63.sp3.S691
- Fabian, A. C., Sanders, J. S., Williams, R. J. R., Lazarian, A., Ferland, G. J., & Johnstone, R. M. (2011, October). The energy source of the filaments around the giant galaxy NGC 1275. *Monthly Notices of the Royal Astronomical Society*, 417(1), 172-177. doi: 10.1111/j.1365-2966.2011.19034.x
- Fite, W. L., Smith, A. C. H., & Stebbings, R. F. (1962, August). Charge Transfer in Collisions Involving Symmetric and Asymmetric Resonance. *Proceedings of the Royal Society of London Series A*, 268(1335), 527-536. doi: 10.1098/rspa.1962.0156
- Fogle, M., Wulf, D., Morgan, K., McCammon, D., Seely, D. G., Draganić, I. N., & Havener, C. C. (2014, April). X-ray-emission measurements following charge exchange between  $C^{6+}$  and  $H_2$ . *Physical Review A*, 89(4), 042705. doi: 10.1103/PhysRevA.89.042705
- Fritsch, W., & Lin, C. D. (1991, April). The semiclassical close-coupling description of atomic collisions: Recent developments and results. *Physics Reports*, 202(1-2), 1-97. doi: 10.1016/0370-1573(91)90008-A
- Fujimoto, R., Mitsuda, K., Mccammon, D., Takei, Y., Bauer, M., Ishisaki, Y., ... Yamasaki, N. Y. (2007, January). Evidence for Solar-Wind Charge-Exchange X-Ray Emission from the Earth's Magnetosheath. *Publications of the Astronomical Society of Japan*, 59, 133-140. doi: 10.1093/pasj/59.sp1.S133
- Galeazzi, M., Chiao, M., Collier, M. R., Cravens, T., Koutroumpa, D., Kuntz, K. D., ... Walsh, B. M. (2014, August). The origin of the local 1/4-keV X-ray flux in both charge exchange and a hot bubble. *Nature*, 512(7513), 171-173. doi: 10.1038/nature13525
- Gloeckler, G., Cain, J., Ipavich, F. M., Tums, E. O., Bedini, P., Fisk, L. A., ... Kallenbach, R. (1998, July). Investigation of the composition of solar and interstellar matter using solar wind and pickup ion measurements with SWICS and SWIMS on the ACE spacecraft. *Space Science Reviews*, 86, 497-539. doi: 10.1023/A:1005036131689
- Greenwood, J. B., Chutjian, A., & Smith, S. J. (2000, January). Measurements of Absolute, Single Charge-Exchange Cross Sections of  $H^+$ ,  $He^+$  and  $He^{2+}$  with  $H_2O$  and  $CO_2$ . *The Astrophysical Journal*, 529(1), 605-609. doi: 10.1086/308254
- Gu, L., Kaastra, J., & Raassen, A. J. J. (2016, April). Plasma code for astrophysical charge exchange emission at X-ray wavelengths. *Astronomy and Astrophysics*, 588, A52. doi: 10.1051/0004-6361/201527615
- Gu, L., Kaastra, J., Raassen, A. J. J., Mullen, P. D., Cumbee, R. S., Lyons, D., & Stancil, P. C. (2015, December). A novel scenario for the possible X-ray line feature at ~3.5 keV. Charge exchange with bare sulfur ions. *Astronomy and Astrophysics*, 584, L11. doi: 10.1051/0004-6361/201527634
- Hinode Review Team, Al-Janabi, K., Antolin, P., Baker, D., Bellot Rubio, L. R., Bradley, L., ... Young, P. R. (2019, October). Achievements of Hinode in the first eleven years. *Publications of the Astronomical Society of Japan*, 71(5), R1. doi: 10.1093/pasj/psz084
- Hui, Y., Schultz, D. R., Kharchenko, V. A., Stancil, P. C., Cravens, T. E., Lisse, C. M., & Dalgarno, A. (2009, September). The Ion-induced Charge-exchange X-ray Emission of the Jovian Auroras: Magnetospheric or Solar Wind Origin? *The Astrophysical Journal Letter*, 702(2), L158-L162. doi: 10.1088/0004-637X/702/2/L158
- Ishi, D., Ishikawa, K., Numazawa, M., Miyoshi, Y., Terada, N., Mitsuda, K., ... Ezo, Y. (2019, January). Suzaku detection of enigmatic geocoronal solar wind charge exchange event associated with coronal mass ejection. *Publications of the Astronomical Society of Japan*, 71(1), 23. doi: 10.1093/pasj/psy142



- Ishikawa, K., Ezoe, Y., Miyoshi, Y., Terada, N., Mitsuda, K., & Ohashi, T. (2013, June). Suzaku Observation of Strong Solar-Wind Charge-Exchange Emission from the Terrestrial Exosphere during a Geomagnetic Storm. *Publications of the Astronomical Society of Japan*, *65*, 63. doi: 10.1093/pasj/65.3.63
- Janev, R. K., & Winter, H. (1985, January). State-selective electron capture in atom-highly charged ion collisions. *Physics Reports*, *117*(5-6), 265-387. doi: 10.1016/0370-1573(85)90118-8
- Kataoka, R., Ebisuzaki, T., Kusano, K., Shiota, D., Inoue, S., Yamamoto, T. T., & Tokumaru, M. (2009, October). Three-dimensional MHD modeling of the solar wind structures associated with 13 December 2006 coronal mass ejection. *Journal of Geophysical Research (Space Physics)*, *114*(A10), A10102. doi: 10.1029/2009JA014167
- Katsuda, S., Tsunemi, H., Mori, K., Uchida, H., Kosugi, H., Kimura, M., ... Yamaguchi, H. (2011, March). Possible Charge-exchange X-ray Emission in the Cygnus Loop Detected with Suzaku. *The Astrophysical Journal*, *730*(1), 24. doi: 10.1088/0004-637X/730/1/24
- Katsuda, S., Tsunemi, H., Mori, K., Uchida, H., Petre, R., Yamada, S., ... Tamagawa, T. (2012, September). High-resolution X-Ray Spectroscopy of the Galactic Supernova Remnant Puppis A with XMM-Newton/RGS. *The Astrophysical Journal*, *756*(1), 49. doi: 10.1088/0004-637X/756/1/49
- Kimura, M., & Lane, N. F. (1987, January). Traveling-molecular-orbital-expansion studies of electron capture in collisions of fully stripped ions ( $Z=6-9$ ) with H and  $H_2$ . *Physical Review A (General Physics)*, *35*(1), 70-78. doi: 10.1103/PhysRevA.35.70
- Koutroumpa, D., Acero, F., Lallement, R., Ballet, J., & Kharchenko, V. (2007, December). OVII and OVIII line emission in the diffuse soft X-ray background: heliospheric and galactic contributions. *Astronomy and Astrophysics*, *475*(3), 901-914. doi: 10.1051/0004-6361:20078271
- Koutroumpa, D., Lallement, R., Kharchenko, V., Dalgarno, A., Pepino, R., Izmodenov, V., & Quémerais, E. (2006, December). Charge-transfer induced EUV and soft X-ray emissions in the heliosphere. *Astronomy and Astrophysics*, *460*(1), 289-300. doi: 10.1051/0004-6361:20065250
- Lallement, R. (2009, March). Some Observations Related to the Origin and Evolution of the Local Bubble/Local ISM. *Space Science Reviews*, *143*(1-4), 427-436. doi: 10.1007/s11214-008-9428-y
- Laming, J. M. (2015, September). The FIP and Inverse FIP Effects in Solar and Stellar Coronae. *Living Reviews in Solar Physics*, *12*(1), 2. doi: 10.1007/lrsp-2015-2
- Lee, T.-G., Hesse, M., Le, A.-T., & Lin, C. D. (2004, July). Charge transfer in slow collisions of  $O^{8+}$  and  $Ar^{8+}$  ions with H (1s) below 2 keV/amu. *Physical Review A*, *70*(1), 012702. doi: 10.1103/PhysRevA.70.012702
- Lepri, S. T., & Zurbuchen, T. H. (2004, January). Iron charge state distributions as an indicator of hot ICMEs: Possible sources and temporal and spatial variations during solar maximum. *Journal of Geophysical Research (Space Physics)*, *109*(A1), A01112. doi: 10.1029/2003JA009954
- Lisse, C. M., Dennerl, K., Englhauser, J., Harden, M., Marshall, F. E., Mumma, M. J., ... West, R. G. (1996, October). Discovery of X-ray and Extreme Ultraviolet Emission from Comet C/Hyakutake 1996 B2. *Science*, *274*(5285), 205-209. doi: 10.1126/science.274.5285.205
- Liu, J., Mao, S., & Wang, Q. D. (2011, July). Charge-exchange X-ray emission of M82:  $K\alpha$  triplets of O VII, Ne IX and Mg XI. *Monthly Notices of the Royal Astronomical Society*, *415*(1), L64-L68. doi: 10.1111/j.1745-3933.2011.01079.x
- Liu, Y., Luhmann, J. G., Müller-Mellin, R., Schroeder, P. C., Wang, L., Lin, R. P., ... Sauvaud, J. A. (2008, December). A Comprehensive View of the 2006



- December 13 CME: From the Sun to Interplanetary Space. *The Astrophysical Journal*, 689(1), 563-571. doi: 10.1086/592031
- McComas, D. J., Bame, S. J., Barraclough, B. L., Feldman, W. C., Funsten, H. O., Gosling, J. T., ... Neugebauer, M. (1998, January). Ulysses' return to the slow solar wind. *Geophysical Research Letters*, 25(1), 1-4. doi: 10.1029/97GL03444
- Mewaldt, R. A., Cohen, C. M. S., Cummings, A. C., Davis, A. J., Labrador, A. W., Leske, R. A., ... Wiedenbeck, M. E. (2008, January). Observations of the December 2006 solar energetic particle events with the Low Energy Telescope (LET) on STEREO. In *International cosmic ray conference* (Vol. 1, p. 107-110).
- Meyer, F. W., Howald, A. M., Havener, C. C., & Phaneuf, R. A. (1985, December). Low-energy total-electron-capture cross sections for fully stripped and H-like projectiles incident on H and H<sub>2</sub>. *Physical Review A*, 32(6), 3310-3318. doi: 10.1103/PhysRevA.32.3310
- Meyer, F. W., Phaneuf, R. A., Kim, H. J., Hvelplund, P., & Stelson, P. H. (1979, February). Single-electron-capture cross sections for multiply charged O, Fe, Mo, Ta, W, and Au ions incident on H and H<sub>2</sub> at intermediate velocities. *Physical Review A*, 19(2), 515-525. doi: 10.1103/PhysRevA.19.515
- Mullen, P. D., Cumbee, R. S., Lyons, D., Gu, L., Kaastra, J., Shelton, R. L., & Stancil, P. C. (2017, July). Line Ratios for Solar Wind Charge Exchange with Comets. *The Astrophysical Journal*, 844(1), 7. doi: 10.3847/1538-4357/aa7752
- Mullen, P. D., Cumbee, R. S., Lyons, D., & Stancil, P. C. (2016, June). Charge Exchange-induced X-Ray Emission of Fe xxv and Fe xxvi via a Streamlined Model. *The Astrophysical Journal Supplement Series*, 224(2), 31. doi: 10.3847/0067-0049/224/2/31
- Nindos, A., Alissandrakis, C. E., Hillaris, A., & Preka-Papadema, P. (2011, July). On the relationship of shock waves to flares and coronal mass ejections. *Astronomy & Astrophysics*, 531, A31. doi: 10.1051/0004-6361/201116799
- Nolte, J. L., Stancil, P. C., Liebermann, H. P., Buenker, R. J., Hui, Y., & Schultz, D. R. (2012, December). Final-state-resolved charge exchange in C<sup>5+</sup> collisions with H. *Journal of Physics B Atomic Molecular Physics*, 45(24), 245202. doi: 10.1088/0953-4075/45/24/245202
- Olson, R. E., & Salop, A. (1977, August). Charge-transfer and impact-ionization cross sections for fully and partially stripped positive ions colliding with atomic hydrogen. *Physical Review A*, 16(2), 531-541. doi: 10.1103/PhysRevA.16.531
- ØStgaard, N., Mende, S. B., Frey, H. U., Gladstone, G. R., & Lauche, H. (2003, July). Neutral hydrogen density profiles derived from geocoronal imaging. *Journal of Geophysical Research (Space Physics)*, 108(A7), 1300. doi: 10.1029/2002JA009749
- Pollock, A. M. T. (2007, March). A new paradigm for the X-ray emission of O stars from XMM-Newton observations of the O9.7 supergiant ζ Orionis. *Astronomy and Astrophysics*, 463(3), 1111-1123. doi: 10.1051/0004-6361:20053838
- Reames, D. V. (1999, October). Particle acceleration at the Sun and in the heliosphere. *Space Science Reviews*, 90, 413-491. doi: 10.1023/A:1005105831781
- Richardson, J. D., Wang, C., Kasper, J. C., & Liu, Y. (2005, January). Propagation of the October/November 2003 CMEs through the heliosphere. *Geophysical Research Letters*, 32(3), L03S03. doi: 10.1029/2004GL020679
- Ringuette, R., Koutroumpa, D., Kuntz, K. D., Kaaret, P., Jahoda, K., LaRocca, D., ... Bluem, J. (2021, September). HaloSat Observations of Heliospheric Solar Wind Charge Exchange. *The Astrophysical Journal*, 918(2), 41. doi: 10.3847/1538-4357/ac0e33
- Robertson, I. P., Collier, M. R., Cravens, T. E., & Fok, M. C. (2006, Decem-

- ber). X-ray emission from the terrestrial magnetosheath including the cusps. *Journal of Geophysical Research (Space Physics)*, *111*(A12), A12105. doi: 10.1029/2006JA011672
- Shibata, K., & Magara, T. (2011, December). Solar Flares: Magnetohydrodynamic Processes. *Living Reviews in Solar Physics*, *8*(1), 6. doi: 10.12942/lrsp-2011-6
- Smith, R. K., Foster, A. R., & Brickhouse, N. S. (2012, April). Approximating the X-ray spectrum emitted from astrophysical charge exchange. *Astronomische Nachrichten*, *333*(4), 301. doi: 10.1002/asna.201211673
- Snowden, S. L., Collier, M. R., & Kuntz, K. D. (2004, August). XMM-Newton Observation of Solar Wind Charge Exchange Emission. *The Astrophysical Journal*, *610*(2), 1182-1190. doi: 10.1086/421841
- Toriumi, S., & Wang, H. (2019, May). Flare-productive active regions. *Living Reviews in Solar Physics*, *16*(1), 3. doi: 10.1007/s41116-019-0019-7
- Tsuru, T. G., Ozawa, M., Hyodo, Y., Matsumoto, H., Koyama, K., Awaki, H., ... Yamasaki, N. Y. (2007, January). X-Ray Spectral Study of the Extended Emission, ‘the Cap’, Located 11.6kpc above the Disk of M82. *Publications of the Astronomical Society of Japan*, *59*, 269-282. doi: 10.1093/pasj/59.sp1.S269
- Tsyganenko, N. A. (1995, April). Modeling the Earth’s magnetospheric magnetic field confined within a realistic magnetopause. *Journal of Geophysical Research*, *100*(A4), 5599-5612. doi: 10.1029/94JA03193
- Tsyganenko, N. A., & Sitnov, M. I. (2005, March). Modeling the dynamics of the inner magnetosphere during strong geomagnetic storms. *Journal of Geophysical Research (Space Physics)*, *110*(A3), A03208. doi: 10.1029/2004JA010798
- Verscharen, D., Klein, K. G., & Maruca, B. A. (2019, December). The multi-scale nature of the solar wind. *Living Reviews in Solar Physics*, *16*(1), 5. doi: 10.1007/s41116-019-0021-0
- Viall, N. M., & Borovsky, J. E. (2020, July). Nine Outstanding Questions of Solar Wind Physics. *Journal of Geophysical Research (Space Physics)*, *125*(7), e26005. doi: 10.1029/2018JA026005
- Walker, S. A., Kosec, P., Fabian, A. C., & Sanders, J. S. (2015, November). X-ray analysis of filaments in galaxy clusters. *Monthly Notices of the Royal Astronomical Society*, *453*(3), 2480-2489. doi: 10.1093/mnras/stv1829
- Walsh, B. M., Niehof, J., Collier, M. R., Welling, D. T., Sibeck, D. G., Mozer, F. S., ... Kuntz, K. D. (2016, March). Density variations in the Earth’s magnetospheric cusps. *Journal of Geophysical Research (Space Physics)*, *121*(3), 2131-2142. doi: 10.1002/2015JA022095
- Wargelin, B. J., Beiersdorfer, P., Neill, P. A., Olson, R. E., & Scofield, J. H. (2005, November). Charge-Exchange Spectra of Hydrogenic and He-like Iron. *The Astrophysical Journal*, *634*(1), 687-697. doi: 10.1086/496874
- Zurbuchen, T. H., & Richardson, I. G. (2006, March). In-Situ Solar Wind and Magnetic Field Signatures of Interplanetary Coronal Mass Ejections. *Space Science Reviews*, *123*(1-3), 31-43. doi: 10.1007/s11214-006-9010-4

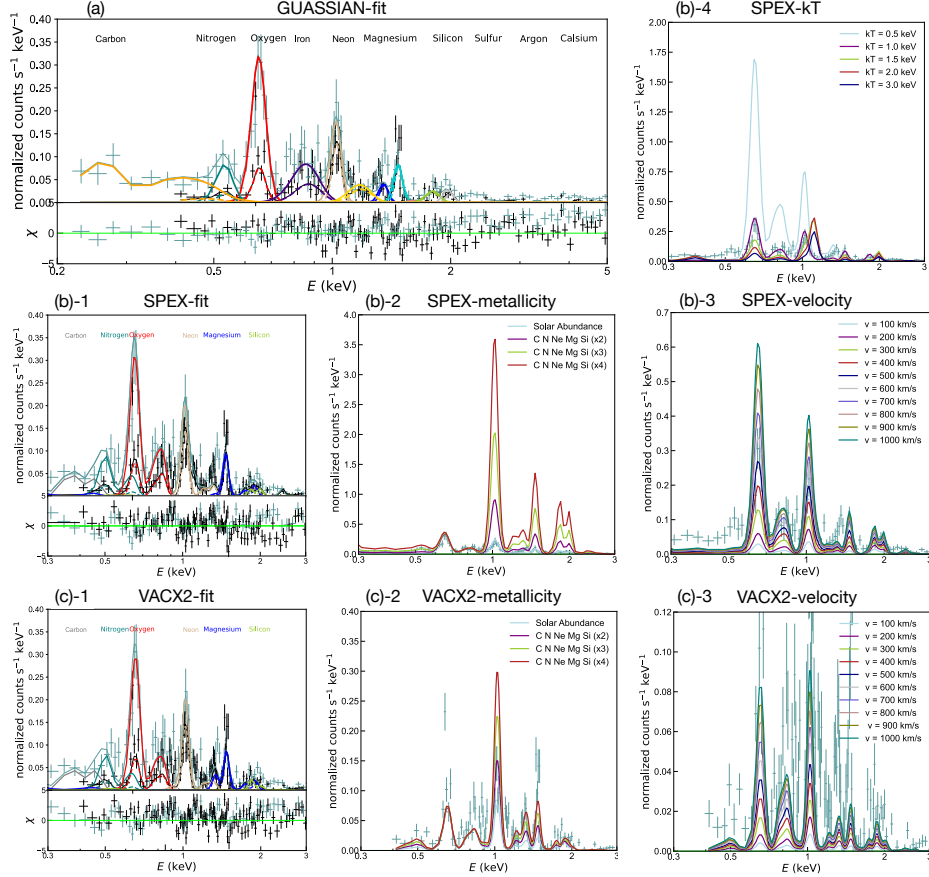


**Figure 3.** (a) Net SWCX spectrum and the fitted Gaussian models for the back-side and front-side illuminated CCDs. *blue* cross: data from XIS1, *black* cross: merged data from XIS0, XIS2, and XIS3. (b)-1 shows the fit of CX model in SPEX. Comparisons of the SPEX-CX model in terms of metal abundance, collisional velocity, and plasma temperature are shown in (b)-2, (b)-3, and (b)-4. Parameters configuration for (b)-2: ionization temperature  $kT = 1.04$  keV and collision velocity  $v = 592.5$  km s<sup>-1</sup>, and solar abundance for elements other than C, N, Ne, Mg, Si; for (b)-3, solar abundance and relative velocity  $v = 592.5$  km s<sup>-1</sup>; for (b)-4, solar abundance and ionization temperature  $kT = 1.04$  keV. (c)-1 shows the fit of VACX2 model incorporated in XSPEC. Comparisons of the XSPEC-VACX2 model in terms of metal abundance and collisional velocity are shown in (c)-2, (c)-3. Parameters configuration for (c)-2: plasma temperature  $kT = 1.05$  keV, and solar abundance for elements other than C, N, Ne, Mg, Si; for (c)-3, solar abundances are set for all elements.

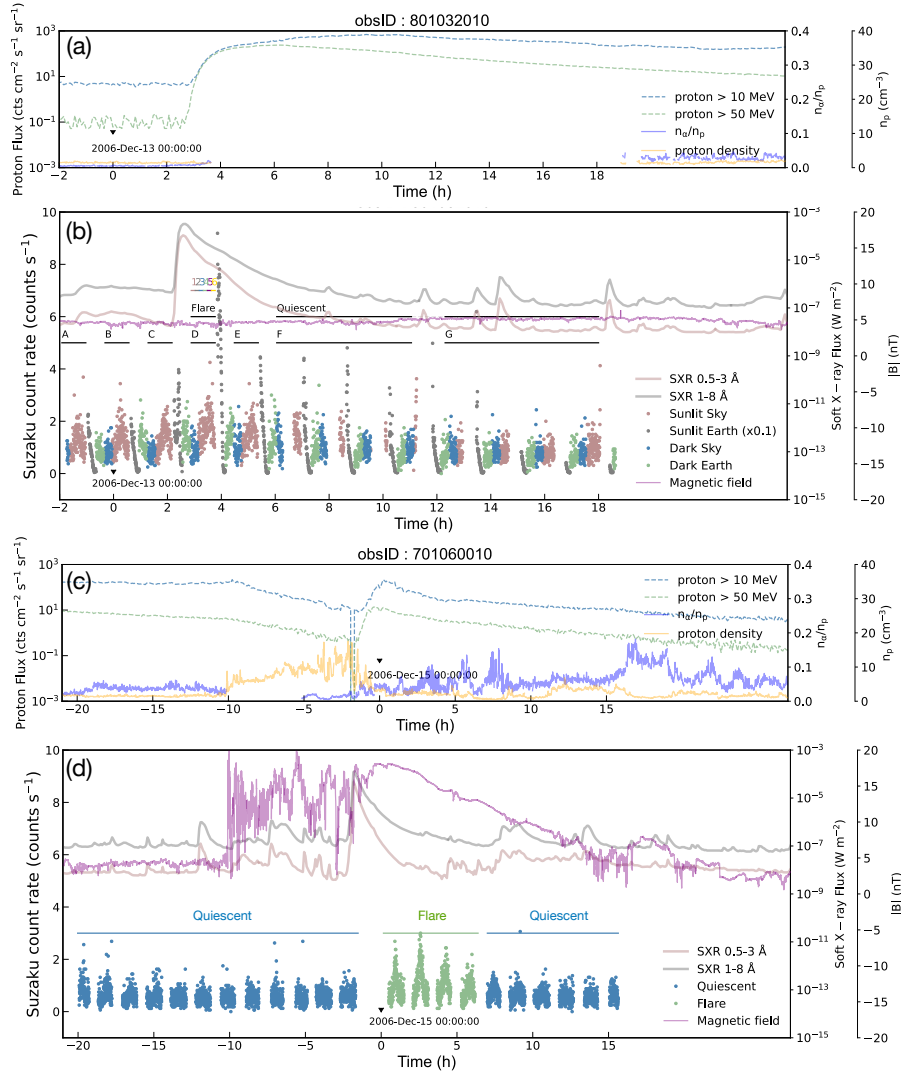


**Figure 4.** The light curves for the Suzaku X-ray background emission and other solar activity tracers. During the observation 801032010/701060010 period: Proton flux observed by GOES satellite, alpha to proton density ratio, and proton density measured by ACE satellite are shown in (a)/(c); Count rate of the Suzaku X-ray background emission, soft X-ray flux measured by GOES satellite, and the magnetic field strength measured by ACE satellite are shown in (b)/(d).

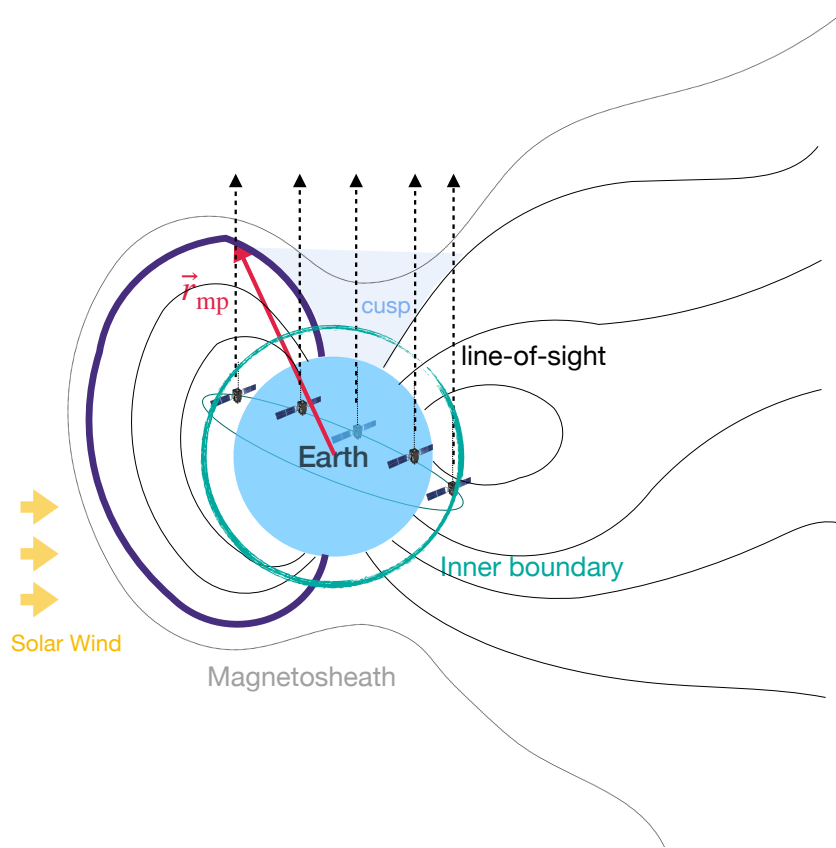


**Figure 5.** A sketch (not drawn to scale) of the Earth, magnetosphere, Suzaku orbit, cusp region, and the definition of  $\vec{r}_{mp}$  where the line of sight meets the last-closed geomagnetic field line.

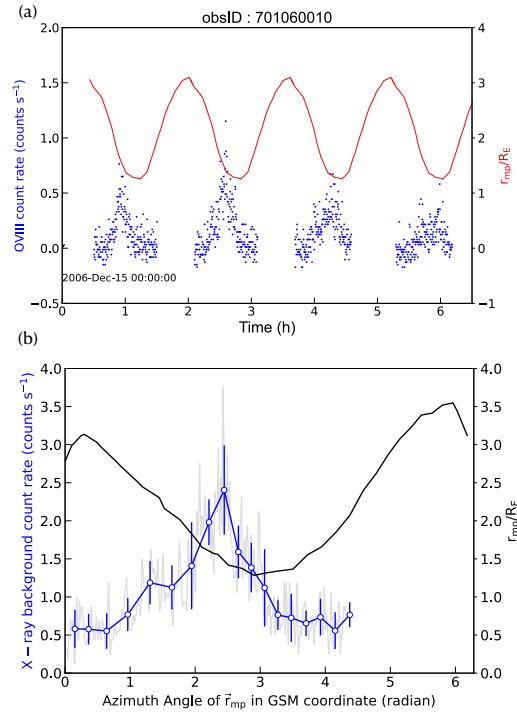


**Figure 6.** (a) Time history of the counting rate for O<sup>7+</sup> emission line, plotted together with  $r_{mp}$ , the radial distance from the Earth center of the position where the magnetic field is open to out space for the first time along the line of site. (b) The X-ray intensity and  $r_{mp}$  plotted as functions of the azimuth angle of the  $r_{mp}$  point in the GSM coordinate. The figure shows only for cycle 2 of (a).